environmental microbiology

Environmental Microbiology (2020) **00**(00), 00–00 doi:10.1111/1462-2920.15344

Sequence analysis and specificity of distinct types of menaquinone methyltransferases indicate the widespread potential of methylmenaquinone production in bacteria and archaea

Dennis Wilkens,[1] Reinhard Meusinger,[2] Sascha Hein[1] and Jörg Simon [1,3]*

[1]*Microbial Energy Conversion and Biotechnology, Department of Biology, Technical University of Darmstadt, Schnittspahnstraße 10, Darmstadt, 64287, Germany.*

[2]*Department of Chemistry, Macromolecular Chemistry, Technical University of Darmstadt, Alarich-Weiss-Str. 4, Darmstadt, 64287, Germany.*

[3]*Centre for Synthetic Biology, Technical University of Darmstadt, Darmstadt, 64283, Germany.*

Summary

Menaquinone (MK) serves as an essential membranous redox mediator in various electron transport chains of aerobic and anaerobic respiration. In addition, the composition of the quinone/quinol pool has been widely used as a biomarker in microbial taxonomy. The HemN-like class C radical SAM methyltransferases (RSMTs) MqnK, MenK and MenK2 have recently been shown to facilitate specific menaquinone methylation reactions at position C-8 (MqnK/MenK) or C-7 (MenK2) to synthesize 8-methylmenaquinone, 7-methylmenaquinone and 7,8-dimethylmenaquinone. However, the vast majority of protein sequences from the MqnK/MenK/MenK2 family belong to organisms, whose capacity to produce methylated menaquinones has not been investigated biochemically. Here, representative putative *menK* and *menK2* genes from *Collinsella tanakaei* and *Ferrimonas marina* were individually expressed in *Escherichia coli* (wild-type or *ubiE* deletion mutant) and the corresponding cells were found to produce methylated derivatives of the endogenous MK and 2-demethylmenaquinone. Cluster and phylogenetic analyses of 828 (methyl)menaquinone methyltransferase sequences revealed signature motifs that allowed to discriminate enzymes of the MqnK/MenK/MenK2 family from other radical SAM enzymes and to identify C-7-specific menaquinone methyltransferases of the MenK2 subfamily. This study will help to predict the methylation status of the quinone/quinol pool of a microbial species (or even a microbial community) from its (meta)genome and contribute to the future design of microbial quinone/quinol pools in a Synthetic Biology approach.

Introduction

Composition and function of microbial quinone/quinol pools

Membranous quinones are essential to the majority of life forms and are firmly established as an important biomarker in microbial taxonomy (Collins and Jones, 1981; Nowicka and Kruk, 2010). In anaerobic environments, the most important quinones are 2-demethylmenaquinone (DMK), menaquinone (MK) and its methylated derivatives 7-methylmenaquinone (7-MMK), 8-methylmenaquinone (8-MMK) and 7,8-dimethylmenaquinone (7,8-DMMK) (Hein *et al*., 2018). A single microorganism can synthesize a variety of quinones that collectively form the quinone/quinol pool in the membrane. Individual quinones take part in one or more distinct electron transport chains involved in aerobic or anaerobic respiration. The standard redox potentials at pH 7 (E_0') of DMK/$DMKH_2$ ($E_0' \approx +40$ mV) and MK/MKH_2 ($E_0' \approx -70$ mV) are more negative compared to E_0' of ubiquinone [UQ; E_0' (UQ/UQH_2) $\approx +100$ mV] and it was determined that each additional methyl group shifted the redox potential to more negative values (Unden and Bongaerts, 1997; Schmidt *et al*., 1999; Hein *et al*., 2018). This feature could facilitate the participation of methylated quinones in 'low-potential electron transport chains' involved in modes of anaerobic respiration that use a terminal electron acceptor with are rather negative redox potential. For example, 8-MMK has been shown to be involved in polysulphide and sulfite respiration [E_0' (polysulfide/

Received 12 October, 2020; accepted 30 November, 2020. **For correspondence. E-mail simon@bio.tu-darmstadt.de; Tel. (+49) 6151 1624680; Fax (+49) 6151 1624643

HS^-) ≈ −270 mV; E_0' (HSO_3^-/HS^-) = −116 mV] (Dietrich and Klimmek, 2002; Eller *et al*., 2019).

The presence of MMK species has been reported for many different microorganisms. However, known MMK-containing microbes belong to only four different phyla, namely Proteobacteria (orders Burkholderiales, Alteromonadales and Campylobacterales), Actinobacteria (orders Eggerthellales and Coriobacteriales), Crenarchaeota (orders Desulfurococcales and Thermoproteales) and Euryarchaeota (orders Thermoplasmatales and Natrialbales) (Hein *et al*., 2017). The production of DMMK was experimentally confirmed only in members of the actinobacterial class Coriobacteriia, for example, in *Adlercreutzia equolifaciens*, which uses MMK and DMMK as main constituents of the quinone/quinol pool (Maruo *et al*., 2008; Hein *et al*., 2018).

Biosynthesis of MK and methylated MK derivatives

The MK molecule is the product of two fundamentally different biochemical pathways: (i) the long-known classical Men pathway as present in Gammaproteobacteria such as *Escherichia coli* and (ii) the more recently described futalosine (or Mqn) pathway as exemplified by *Streptomyces coelicolor* A3(2) (Hiratsuka *et al*., 2008; Dairi, 2012). The synthesis of MMK needs an additional methylation step, which is catalyzed by one of the dedicated class C radical SAM methyltransferases (RSMTs) designated MqnK, MenK or MenK2 (Hein *et al*., 2017, 2018). Typically, members of the MqnK/MenK/MenK2 family have a mass of 48–54 kDa. They share a similar domain structure consisting of a short N-terminal so-called trip-wire connected to the catalytic domain, a linker domain and a C-terminal HemN domain (Supporting Information Fig. S1). The latter is named after the biochemically characterized coproporphyrinogen III oxidase HemN, which catalyzes the oxygen-independent decarboxylation of two propionate side chains in haem biosynthesis (Layer et al., 2003, 2006; Broderick *et al*., 2014; Hein *et al*., 2018; Jin *et al*., 2018). Thus, in contrast to class C RSMTs, HemN does not catalyse a methylation reaction.

The catalytic domain of class C RSMTs consists of a $\beta_8\alpha_8$ TIM-barrel fold with a strictly conserved CxxxCxxC motif that ligates a [4Fe-4S] centre (Wang *et al*., 2014). Furthermore, HemN has been shown to harbour two SAM molecules (SAM1 and SAM2) at different binding sites and it is thought that this feature generally applies to class C RSMTs (Layer *et al*., 2003, 2006; Zhang *et al*., 2017; Ji *et al*., 2019). SAM1 was proposed to be cleaved into a 5′-deoxyadenosyl radical and methionine upon reduction with an electron provided by a small electron carrier (a ferredoxin or flavodoxin) that is transferred via the [4Fe-4S] centre. Subsequently, the 5′-deoxyadenosyl radical is likely to abstract a hydrogen atom from the methyl group of SAM2 (or an amino acid residue that had been methylated before by SAM2), thereby generating a methylene radical. Finally, this radical, an electron and a proton are transferred to the substrate. Such a scenario has been proposed previously for MqnK/MenK/MenK2-type enzymes (Hein *et al*., 2017).

MqnK/MenK and MenK2 catalyze similar reactions but methylate the naphthoquinone group of MK at different positions. MqnK/MenK enzymes have been generally suggested to methylate menaquinone specifically at position C-8 to obtain 8-MMK, while MenK2 has been envisaged to specifically methylate MK at position C-7 to produce 7-MMK (Hein *et al*., 2017, 2018). Previously, the MenK proteins from *Adlercreutzia equolifaciens* and *Shewanella oneidensis* were individually produced in *Escherichia coli* and shown to promote the production of 8-MMK_8 and 8-methyl-2-demethylmenaquinone (8-$MDMK_8$) (Hein *et al*., 2017). Furthermore, the *mqnK* gene of *Wolinella succinogenes* was shown to be required for 8-MMK_6 biosynthesis, and the MK methylation activity of *A. equolifaciens* MenK was demonstrated using an *in vitro* assay (Hein *et al*., 2017). The *A. equolifaciens* MenK2 protein was shown to be required for the synthesis of 7-MMK_6 and 7,8-$DMMK_6$ when produced in *W. succinogenes* as well as for the production of 7-MMK_8 in *E. coli* cells following heterologous production of a strep-tagged derivative (Hein *et al*., 2018). Thus, for the synthesis of 7,8-DMMK, both MqnK and MenK2 were needed, indicating site-specificity of the tested enzymes (Hein *et al*., 2018).

In previous studies, the genome sequences of experimentally proven MMK- and/or DMMK-producing microbial species were checked whether they contained *mqnK*/*menK* and/or *menK2* genes and it turned out that this was indeed the case for all bacteria and the majority of the crenarchaeal species (Hein *et al*., 2017, 2018). Here, 828 putative MqnK/MenK/MenK2 sequences from 297 different microorganisms (753 microbial strains) were retrieved from protein sequence data banks and analysed in order to predict the potential of the corresponding cells to produce methylated MK derivatives, irrespective of whether or not this capacity had been investigated biochemically before. Several signature motifs were specified and one of those allowed to discriminate between MqnK/MenK and MenK2 proteins. As *proof of concept*, the putative MenK and MenK2 proteins from the Actinobacterium *Collinsella tanakaei* as well as MenK from the Gammaproteobacterium *Ferrimonas marina* were produced in *E. coli* and the composition of the respective quinone/quinol pools was analysed.

Results

Cluster analysis of HemN-like radical SAM enzymes and characterization of the MqnK/MenK/MenK2 cluster

A set of 56 957 related protein sequences was retrieved from a PSI-BLAST analysis using 12 class C RSMTs as seed sequences (see *Experimental procedures* for details). To restrict the protein sequences to radical SAM enzymes, the enzyme set was analysed for the presence of the motif Y/VxGGGT, which, when present, is strictly conserved in each of the experimentally characterized MK methyltransferases. The resulting enzyme set of 14 365 sequences was subjected to a CLANS analysis and thereby divided into 15 clusters, each containing between 31 and 7744 sequences (Fig. 1A and Table 1). The eight largest clusters were named after the enzymes HemW, HemZ, ChuW, HutW, MqnK/MenK/MenK2, Jaw5, NosN and C10P (Fig. 1B and Table 1; note that this assignment was based on the 12 seed class C RSMTs and 10 other characterized radical SAM proteins). A Bayesian phylogenetic analysis of 23 selected HemN-like class C RSMTs was found to coincide with the CLANS analysis (Fig. 2).

The MqnK/MenK/MenK2 cluster comprised 819 bacterial and 9 archaeal sequences from an 'archaeal MqnK' subcluster (Fig. 1B). These 828 sequences derived from 297 different species (763 individual strains) from 14 established and 4 candidate phyla, and 237 of these species have been assigned to taxonomic families (Fig. 3 and Supporting Information Table S1). To the best of our knowledge, however, the presence of MMK and/or

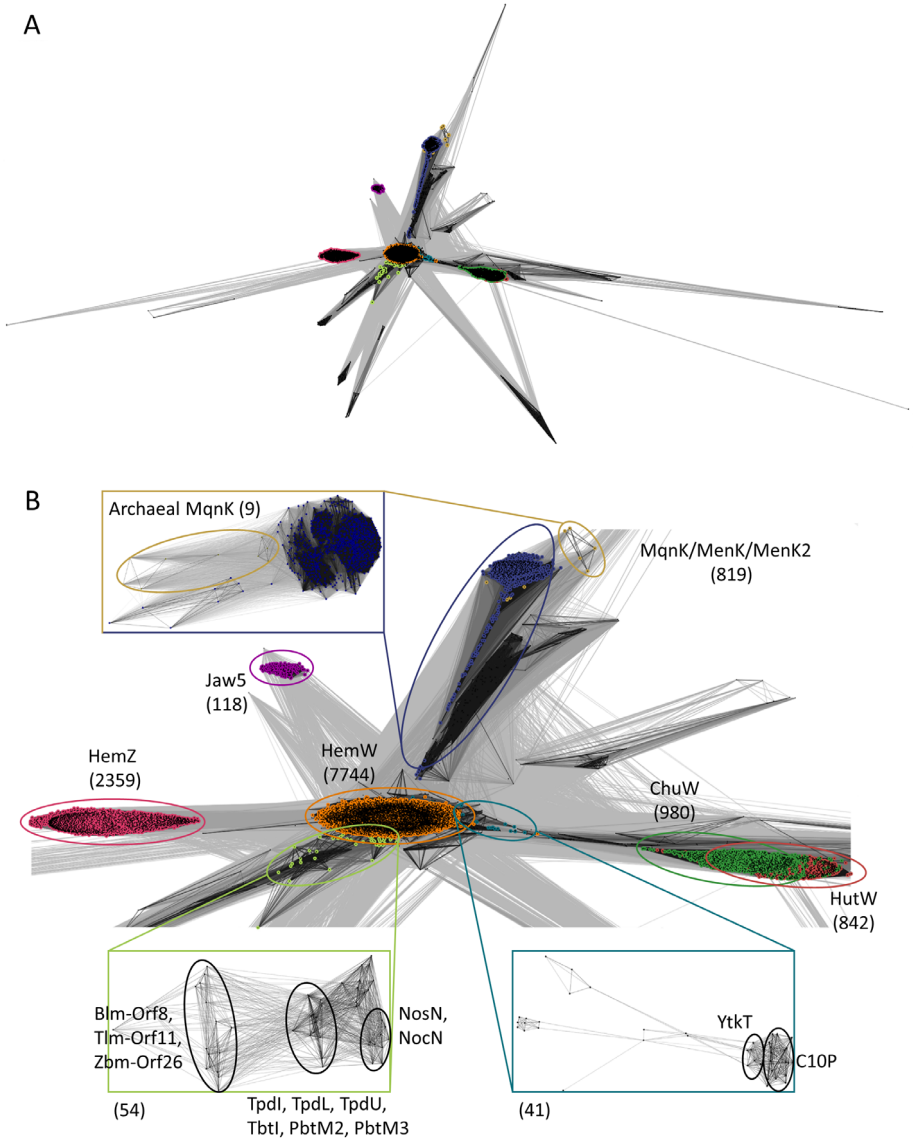

Fig. 1. Cluster analysis of 14 365 sequences of HemN-like radical SAM enzymes using CLANS.
A. Overview with each point representing a single sequence and each line visualizing the *p*-value between two points. Dark lines represent a high pairwise similarity (low *p*-value) and lighter lines a lower pairwise similarity (high *p*-value) closer to the cut off value of 10^{-45}. Each cluster is highlighted with a different colour.
B. Close-up with cluster designations. The insets depict individual cluster analyses of the MqnK/MenK/MenK2, NosN and C10P subclusters (cut off value 10^{-80}).

Table 1. The presence of signature motifs in protein sequences constituting the eight largest radical SAM enzyme clusters of the CLANS analysis.

	Cluster [a]							
Domain and signature motif	HemW [b] (7744)	HemZ [c] (2359)	ChuW [d] (980)	HutW [d] (842)	MKMT [e] (828)	Jaw5[f] (118)	NosN [g] (54)	C10P [h] (41)
Catalytic domain								
LYxHxPFCxxxCxxCxF	2278	6	324	783	795	0	0	5
YFxxxRxE	11	0	0	0	759	1	8	0
GxxFxxxYxGGGT	49	1	2	9	772	0	0	1
RxSxGxQxFxxxxL	5959	0	0	0	801	0	45	32
Linker domain								
QxTxYPLx	0	0	0	0	743	0	0	3
NxFxxxxY	158	25	10	388	787	0	14	0

[a]The number in parentheses denotes the number of sequences considered in the CLANS analysis.
[b]HemW from *Lactococcus lactis* functions as a haem chaperone (Abicht *et al*., 2012). 47% of the cluster sequences have been annotated as HemW, 38% as HemN, 6% as hypothetical proteins and 1% as 'radical SAM protein'.
[c]HemZ is the ferrochelatase that synthesizes haem *b* from protoporphyrin IX (Homuth *et al*., 1999; Parish *et al*., 2005); 43% of the cluster sequences have been annotated as HemZ and 44% as 'coproporphyrinogen III oxidase'.
[d]ChuW/HutW are class C RSMT enzymes and annotated as such in 89% of the total of 1822 sequences (Sofia *et al*., 2001). The enzymes catalyse oxygen-independent heme degradation by opening and methylating the porphyrin ring to yield an open tetrapyrrole (LaMattina *et al*., 2016).
[e]The menaquinone methyltransferase (MKMT) cluster comprises MqnK, MenK and MenK2 enzymes; 89% of the cluster sequences have been annotated as 'coproporphyrinogen III oxidase'.
[f]Jaw5 is involved in the synthesis of the antifungal agent jawsamycin by *Streptoverticillium fervens* HP-891 (now *Streptomyces roseoverticillatus*) (Watanabe *et al*., 2006a, b); 74% of the cluster sequences have been annotated as 'radical SAM protein'.
[g]The NosN cluster contains enzymes annotated as NosN, NocN, Blm-Orf8, Tlm-Orf11, Zbm-Orf26, TpdI, TpdL, TpdU, TbtI, PbtM2 and PbtM3 (Du *et al*., 2000; Tao *et al*., 2007; Galm *et al*., 2009; Morris *et al*., 2009; Yu *et al*., 2009; Ding *et al*., 2010; Tocchetti *et al*., 2013; Burkhart *et al*., 2017; Mahanta *et al*., 2017; Zhang *et al*., 2017). These enzymes are (potentially) involved in the production of various antibiotics such as nosiheptide, thiomuracin, GE2270, bleomycin, zorbamycin and tallysomycin.
[h]This cluster comprises C10P (involved in the synthesis of the natural product CC-1065 and its homologue YtkT, which is involved in yatakemycin production (MacMillan and Boger, 2009; Huang *et al*., 2012; Wu *et al*., 2017).

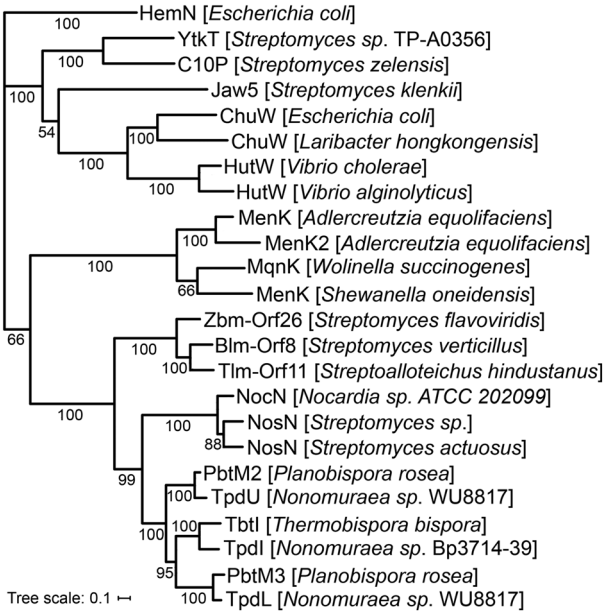

Fig. 2. Phylogenetic analysis of 23 HemN-like class C RSMTs used in the cluster analysis including *Ec*HemN as outlier. The underlying multiple sequence alignment was calculated with ClustalX and the dendrogram was constructed with MrBayes. Sequences of the HemW and HemZ clusters were disregarded since these enzymes do not catalyse methylation reactions. The scale bar shows 0.1 estimated substitutions per site.

DMMK has been shown biochemically for only 63 species including one eukaryotic organism (Supporting Information Table S2). Of those, the bacterial and archaeal species belong to only four different phyla, namely Proteobacteria, Actinobacteria, Crenarchaeota and Euryarchaeota, but only 39 of the 828 sequences mentioned above originated from biochemically confirmed MMK/DMMK-containing organisms (Supporting Information Table S1) (Hein *et al*., 2017, 2018). The 41 MenK2 enzymes (see below for classification criteria) were found exclusively in the families Coriobacteriaceae and Eggerthellaceae (class Coriobacteriia; phylum Actinobacteria) and each of the corresponding genomes encoded a canonical MenK enzyme as well (Hein *et al*., 2018). Despite the presence of *mqnK* or *menK* genes, the synthesis of methylated MK derivatives has not been reported for any of the organisms grouped in the phyla *Candidatus* Bathyarchaeota, *Candidatus* Altiarchaeota, *Candidatus* Coatesbacteria, *Candidatus* Dadabacteria, Verrucomicrobia, Planctomycetes, Spirochaetes, Lentisphaerae, Elusimicrobia, Bacteroidetes, Aquificae, Deinococcus-Thermus, Deferribacteres, Chloroflexi and Firmicutes (Fig. S3; see Supporting Information Table S1 for a list of corresponding validated species).

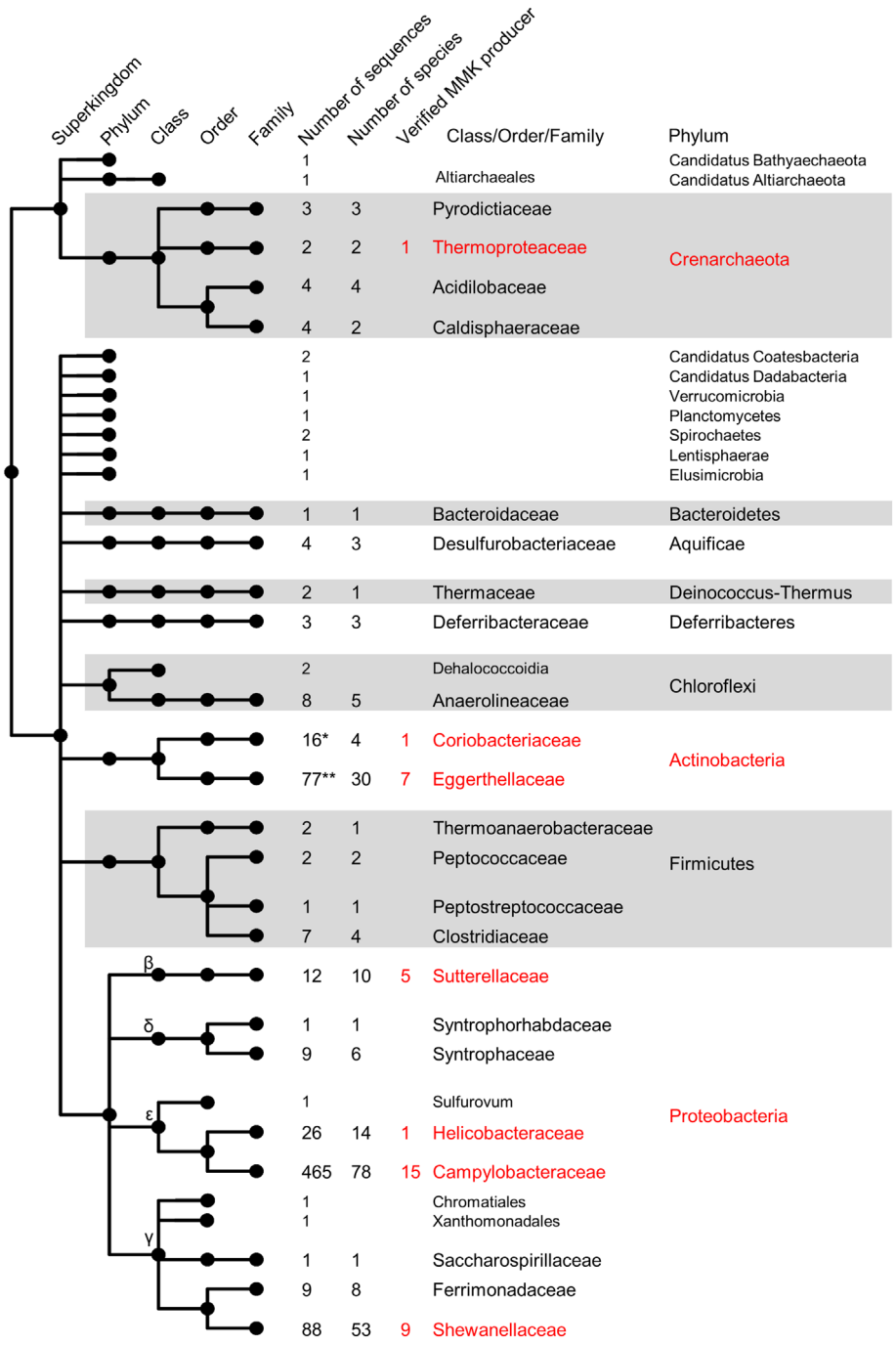

Fig. 3. Phylogenetic distribution of 763 non-identical protein sequences of the MqnK/MenK/MenK2 family from 237 different species. MMK production has been shown biochemically for only 39 of these species (red numbers). The names of the corresponding families and phyla are also given in red. See Supporting Information Tables S1 and S2 for further details. *7 out of 16 sequences belong to MenK2 proteins; **31 out of 77 sequences belong to MenK2 proteins.

Identification of signature motifs in sequences of MqnK/MenK/MenK2 cluster enzymes

Within the 828 MqnK/MenK/MenK2 cluster sequences, six signature motifs, located in the catalytic or the linker domain, were manually identified (Table 1; Supporting Information Fig. S1). Two of these motifs (YFxxxRxE; QxTxYPLx) were found almost exclusively in members of the MqnK/MenK/MenK2 cluster and nine variants of the QxTxYPLx motif were used to define subgroups of the MqnK/MenK/MenK2 cluster (Fig. 4; Supporting Information Fig. S8). Of those, the most abundant motif proved to be QxTxYPLM, which was present in 88% of the sequences. Interestingly, each of the 41 MenK2 sequences contained a distinct motif variant (QxTxSPLY), in which the C-terminal tyrosine served as indicative residue (Fig. 4). As deduced from homology

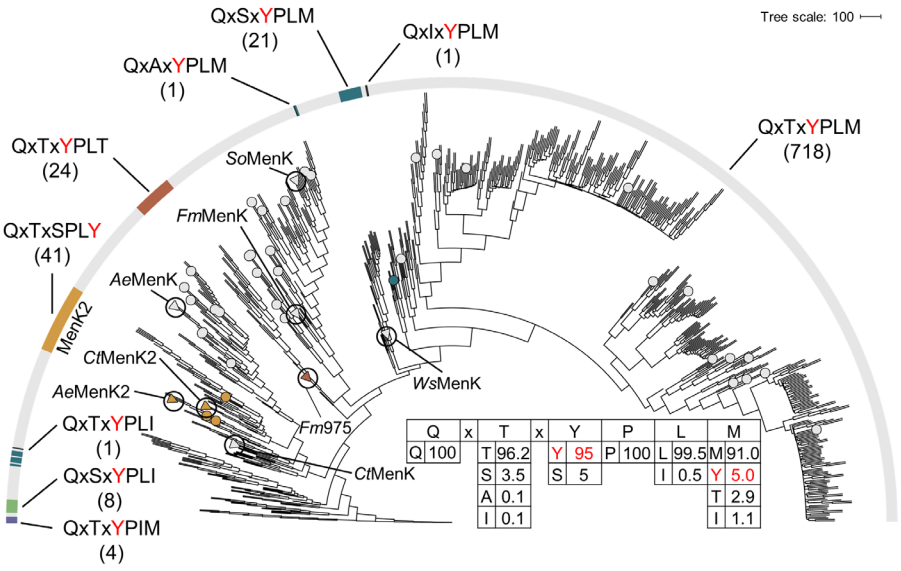

Fig. 4. Bootstrap consensus tree of 819 bacterial sequences from the MqnK/MenK/MenK2 cluster and distribution of the QxTxYPLx signature motif. Dots represent enzymes from experimentally characterized MMK-producing species, such as *A. equolifaciens* (*Ae*), *S. oneidensis* (*So*) and *W. succinogenes* (*Ws*). Triangles represent the enzymes from *F. marina* (*Fm*) and *C. tanakaei* (*Ct*) that were investigated in this study. The colour at the encompassing semicircle refers to the nine variants of the QxTxYPLx motif and the position of all (putative) MenK2 enzymes is pointed out. Numbers below the motifs indicate the corresponding number of sequences. The table illustrates the frequency distribution of individual amino acids within the QxTxYPLx motif (given in percentages for each position). The scale bar shows 100 bootstrap partitions.

models, the respective QxTxYPLM and QxTxSPLY motifs of MenK and MenK2 from *Collinsella tanakei* are located near the putative (M)MK binding site in the vicinity of SAM2 (Fig. 5). Thus, it appears conceivable that the tyrosine to serine and methionine to tyrosine transitions could influence the specificity of the menaquinone methylation site at position C-7 or C-8.

Production and functional characterization of MenK/MenK2 homologues from C. tanakaei *and* F. marina

As stated in the Introduction, several members of the phylum Actinobacteria (class Coriobacteriia) are known for the presence of MenK and MenK2 isoenzymes and the resulting production of 7,8-DMMK$_6$ (Hein *et al*., 2018). For example, the genome of the Actinobacterium *C. tanakaei* predicts homologues of MenK and MenK2 (*Ct*MenK, signature motif QxTxYPLM, and *Ct*MenK2, signature motif QxTxSPLY) (Fig. 4). Therefore, *Ct*MenK belongs phylogenetically to a clade of putative C-8-specific methyltransferases although it is closely related to the MenK2 subfamily (Fig. 4). To the best of our knowledge, however, the presence of respiratory quinones in *C. tanakaei* has not been reported before (Nagai *et al*., 2010). Surprisingly, the genome of the Gammaproteobacterium *F. marina* also encodes two putative menaquinone methyltransferases. Both of them belong to the MenK-type and are designated here *Fm*MenK (signature motif QxTxYPLM) and *Fm*975 (signature motif QxTxYPLT) (Fig. 4). Cells of *F. marina* have been described to contain only MK$_7$, ubiquinone-7 and ubiquinone-8 when grown in a complex medium containing peptone and yeast extract (Katsuta *et al*., 2005).

Using a previously established expression system, the four putative (methyl)menaquinone methyltransferases were produced in *E. coli* BL21 (DE3) and roughly similar amounts of C-terminally Strep-tagged *Ct*MenK, *Ct*MenK2, *Fm*MenK and *Fm*975 were detected in corresponding cells by Western blot analysis (Supporting Information Fig. S2A). The presence of *Fm*MenK in *E. coli* BL21 (DE3) gave rise to the production of one quinone species (retention time 14.5 min) in addition to the endogenous MK$_8$ and DMK$_8$ (Fig. 6A–C). Using the methodology reported previously by Hein *et al*. (2017), this quinone was identified as 8-MMK$_8$ confirming that the enzyme from *F. marina* is a functional MenK (Fig. 6D). For unknown reasons, the successful heterologous production of *Fm*975 did not result in the detectable production of a methylated MK$_8$ species (Supporting Information Fig. S2C). Therefore, this protein was potentially inactive and a functional assignment to MK methylation was not possible.

As expected, the quinone profile of *E. coli* BL21 (DE3) cells producing *Ct*MenK2 exhibited 7-MMK$_8$ (retention time 13.3 min; note that the possible formation of 7-MDMK$_8$ could not be confirmed since its retention time is similar to that of MK$_8$) (Fig. 6E and F). In contrast, the production of *Ct*MenK in *E. coli* BL21 (DE3) cells resulted in the presence of four novel quinones as compared with control cells, while DMK$_8$ was not detected (Fig. 6G). The additional quinone with the highest intensity eluted after a retention time of 14.6 min from the HPLC column and showed the indicative UV–Vis absorption spectrum of 8-MMK$_8$ (not shown). At a retention time of 17.3 min, a dimethylated MK derivative eluted that was identified as 5,8-DMMK$_8$ by NMR (Supporting Information Figs. S3, S6 and S7) and mass spectrometry (Supporting

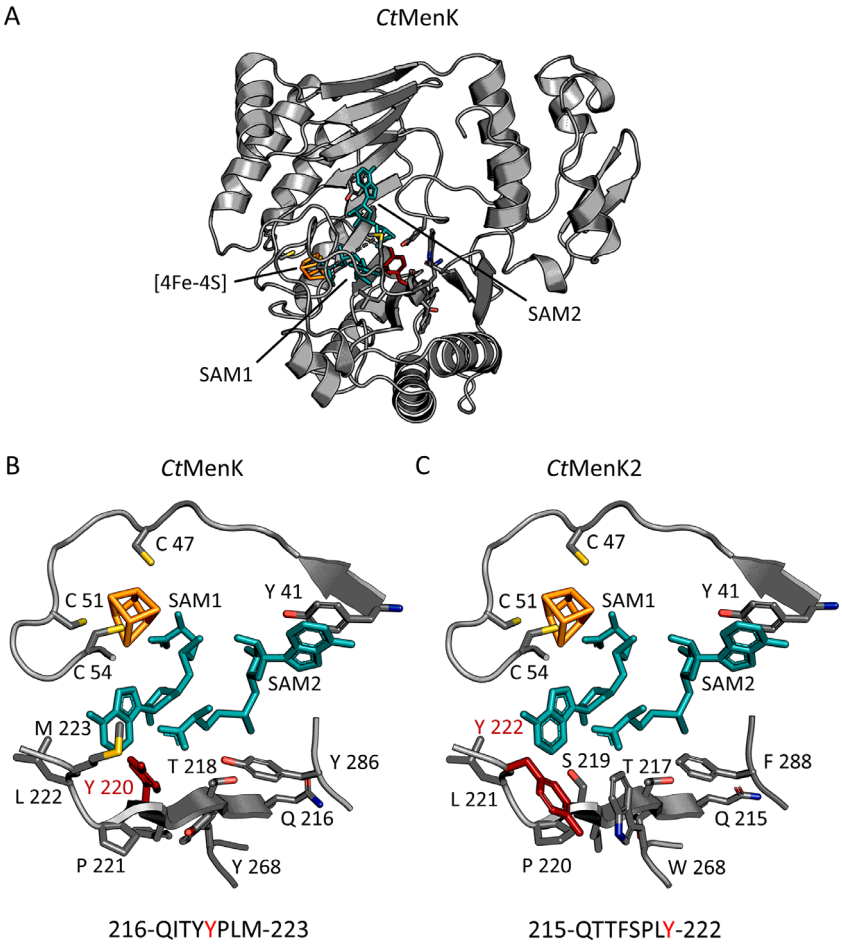

Fig. 5. Homology models of MenK and MenK2 from *C. tanakaei* based on the *E. coli* HemN structure.
A. Full view of *C. tanakaei* MenK (*Ct*MenK) displaying the [4Fe-4S] cluster and the two SAM molecules (SAM1 and SAM2).
B. Putative binding site for (methyl)menaquinone of *Ct*MenK. The QxTxYPLx motif is shown at the bottom.
C. Corresponding view for *C. tanakaei* MenK2 (*Ct*MenK2).

Information Fig. S4). The UV–Vis absorption spectrum of this quinone revealed three peaks at 251 nm, 261 nm and 357 nm (Fig. 6H) with the latter peak being indicative of double methylation [see below and note that the corresponding maximum (349 nm) of the previously described 7,8-DMMK$_8$ was clearly dissimilar] (Hein *et al*., 2018). Two more quinone species were detected with respective retention times of 10.7 and 12.7 min, which were identified as 8-MMK$_7$ and 5,8-DMMK$_7$ based on their UV–Vis and mass spectra (not shown). 7-MMK$_8$ was not detected. These results suggested that *Ct*MenK methylated MK$_8$ at position C-8 and, surprisingly, that the enzyme was apparently able to methylate the resulting 8-MMK$_8$ at position C-5 in a second methylation step, resulting in the synthesis of 5,8-DMMK$_8$.

Methylation of DMK$_8$ by Fm*MenK,* Ct*MenK and* Ct*MenK2 and characterization of 7-MDMK, 8-MDMK and 5,8-DMDMK*

From the results presented above, the question arose whether *Ct*MenK and *Ct*MenK2 were able to methylate DMK$_8$ in the same way as MK$_8$. However, only minor amounts of DMK$_8$ were detected in cells of *E. coli* BL21 (DE3) (Fig. 6A). Moreover, it was known that mono- and dimethylated DMK species eluted close to MK and MMK species in the utilized HPLC setup. Therefore, an *E. coli* BL21 (DE3) mutant was constructed that lacked the *ubiE* gene (see *Experimental procedures* for details). The C-methyltransferase UbiE catalyses methylation reactions at C-3 of ubiquinone and C-2 of MK (Lee *et al*., 1997). As expected, the resulting mutant *E. coli* BL21 (DE3) Δ*ubiE* produced DMK$_8$ but lacked MK$_8$ (Fig. 7A and B). The presence of *Fm*MenK or *Ct*MenK2 in this mutant led to the production of 8-MDMK$_8$ and 7-MDMK$_8$ respectively (Fig. 7C–F). In addition to UV/Vis spectroscopy, 8-MDMK$_8$ and 7-MDMK$_8$ were subjected to mass spectrometry and the presence of an additional methyl group was confirmed (Supporting Information Fig. S4). Upon synthesis of *Ct*MenK the corresponding *E. coli* BL21 (DE3) Δ*ubiE* cells formed at least four DMK derivatives (Fig. 7G). Prominent HPLC peaks were caused by 8-MDMK$_8$ and 5,8-DMDMK$_8$ (Fig. 7F and H; Supporting Information Fig. S4) while minor peaks were attributed to 8-MDMK$_7$ and

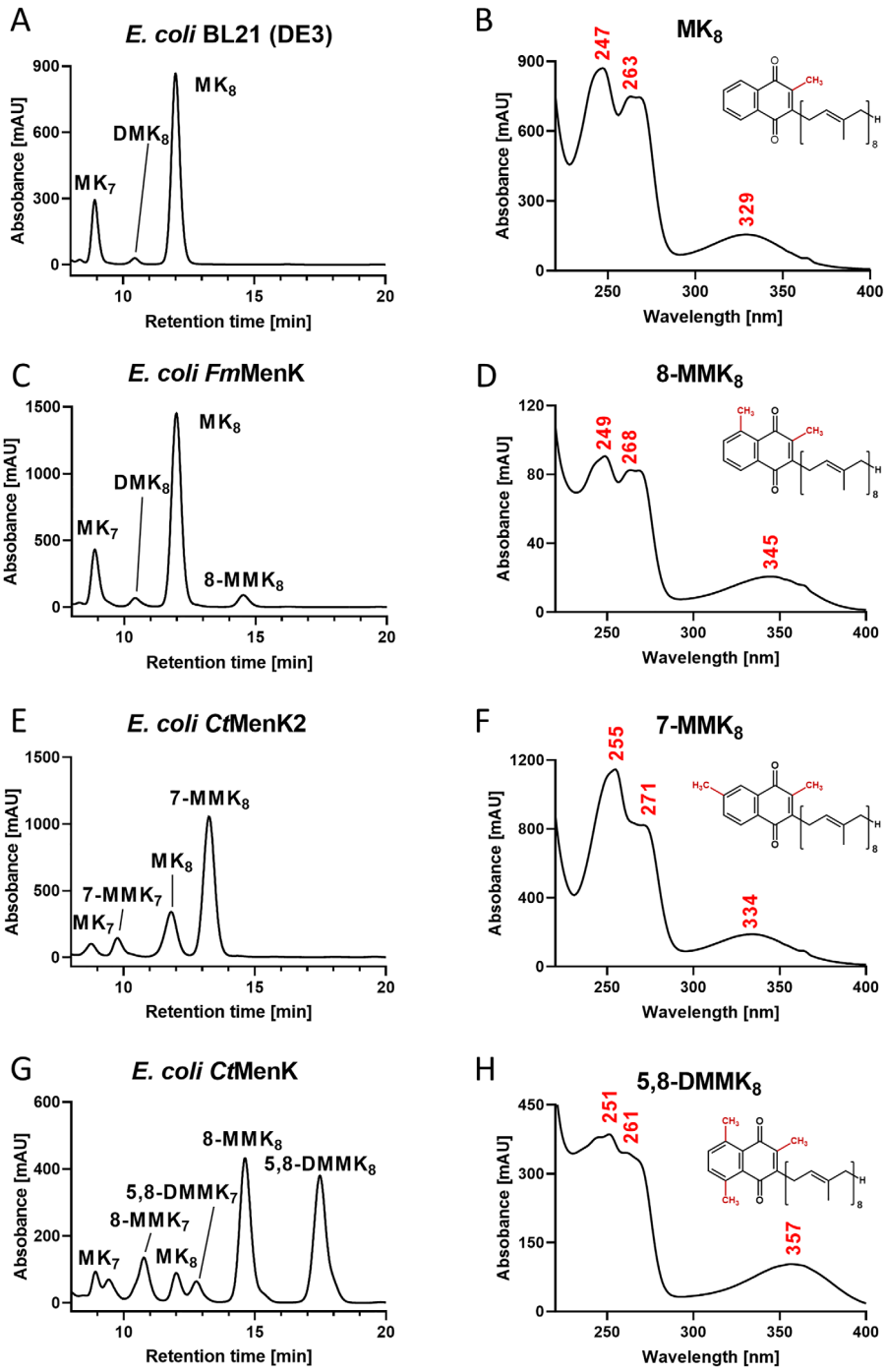

Fig. 6. Analysis of quinones produced in *E. coli* BL21 (DE3) cells.
A. HPLC chromatogram of purified quinones from *E. coli* BL21(DE3).
B. UV/Vis absorption spectrum of MK_8 purified from *E. coli* BL21(DE3).
C. HPLC chromatogram of purified quinones from *E. coli Fm*MenK.
D. UV/Vis absorption spectrum of 8-MMK_8 purified from *E. coli Fm*MenK.
E. HPLC chromatogram of purified quinones from *E. coli Ct*MenK2.
F. UV/Vis absorption spectrum of 7-MMK_8 purified from *E. coli Ct*MenK2.
G. HPLC chromatogram of purified quinones from *E. coli Ct*MenK.
H. UV/Vis absorption spectrum of 5,8-$DMMK_8$ purified from *E. coli Ct*MenK.

5,8-$DMDMK_7$ (Supporting Information Fig. S5). Thus, it appeared that *Fm*MenK, *Ct*MenK and *Ct*MenK2 methylated MK and DMK substrates in the same way. It is notable that the broad absorption peak in the range between 329 nm and 360 nm appears to be a characteristic feature for methylations of the MK and DMK benzenoid rings resulting in a red-shifted maximum with an increasing number of methyl groups (Figs. 6 and 7). The methyl group at C-2 apparently caused the absorption peak/shoulder between 261 and 271 nm, which is less notable or almost absent in DMK species (Figs. 6 and 7).

Discussion

The results indicate that many microbial cells have the potential to synthesize methylated MK derivatives and that this capacity can be predicted from a given genome sequence. In addition to the analysis of full-length protein

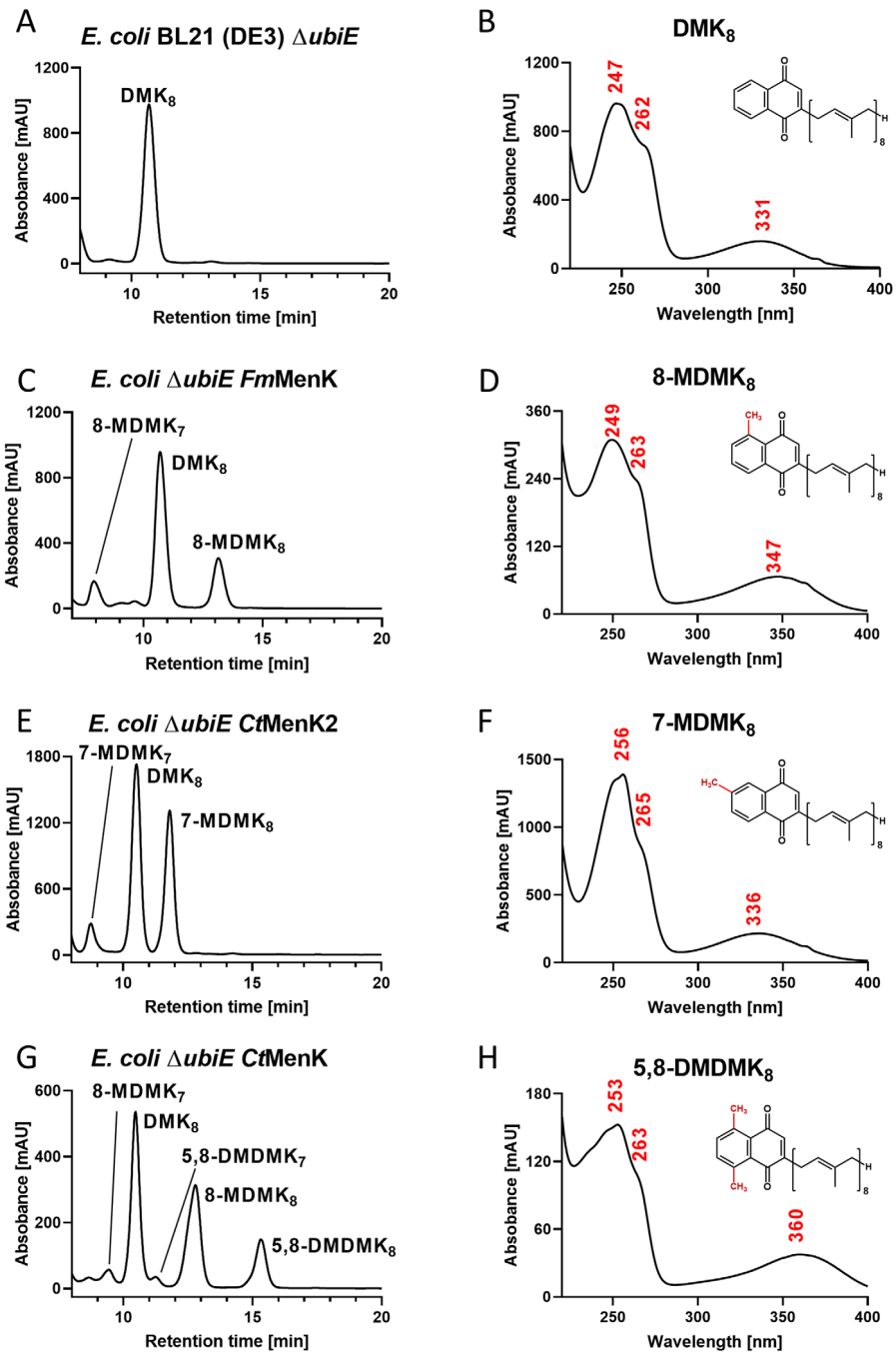

Fig. 7. Analysis of quinones produced in *E. coli* BL21 (DE3) Δ*ubiE* cells.
A. HPLC chromatogram of purified quinones from *E. coli* BL21(DE3) Δ*ubiE*.
B. UV/Vis absorption spectrum of DMK_8 purified from *E. coli* BL21(DE3) Δ*ubiE*.
C. HPLC chromatogram of purified quinones from *E. coli* Δ*ubiE Fm*MenK.
D. UV/Vis absorption spectrum of 8-$MDMK_8$ purified from *E. coli* Δ*ubiE Fm*MenK.
E. HPLC chromatogram of purified quinones from *E. coli* Δ*ubiE Ct*MenK2.
F. UV/Vis absorption spectrum of 7-$MDMK_8$ purified from *E. coli* Δ*ubiE Ct*MenK2.
G. HPLC chromatogram of purified quinones from *E. coli* Δ*ubiE Ct*MenK.
H. UV/Vis absorption spectrum of 5,8-$DMDMK_8$ purified from *E. coli* Δ*ubiE Ct*MenK.

sequences, the presented signature motifs are useful to discriminate members of the MqnK/MenK/MenK2 family from other radical SAM enzymes and to identify MenK2 homologues within the family on the basis of a single signature motif. This is especially helpful since automated systematic annotation in public databases has led to many functional misannotations of class C RSMT enzymes (Schnoes *et al*., 2009). For example, 47% of the 14 365 proteins used in the cluster analysis have been annotated as coproporphyrinogen III oxidases due to their high sequence similarity to HemN and the fact that *E. coli* HemN has been extensively characterized.

Methylation site specificity and discrimination between MqnK/MenK and MenK2 enzymes

As expected, the gammaproteobacterial MenK from *F. marina* catalyzed methylation of MK_8 and DMK_8 in *E. coli* specifically at position C-8. Similar results have been obtained previously when the MenK proteins from

the Actinobacterium *Adlercreutzia equolifaciens* or the Gammaproteobacterium *Shewanella oneidensis* were heterologously produced in *E. coli* (Hein *et al*., 2017). Furthermore, the MqnK protein from *Wolinella succinogenes* was shown to produce specifically 8-MMK_6 (Hein *et al*., 2017). In contrast, the actinobacterial MenK from *C. tanakaei* was apparently able to catalyse two individual methylation reactions at positions C-8 and C-5 of MK_8 and DMK_8 in *E. coli*, which resulted in the production of 8-MMK_8, 8-$MDMK_8$, 5,8-$DMMK_8$ and, most likely, 5,8-$DMDMK_8$. On the other hand, C-7-methylation was not detected, which makes sense in the light of the fact that *C. tanakaei* contains a C-7-specific MenK2 enzyme. Previously, the MenK2 from *A. equolifaciens* was reported to be active in *E. coli* and *W. succinogenes* where it was shown to synthesize 7-MMK_8 and 7-MMK_6, respectively (Hein *et al*., 2018). Hence, the results presented here confirm the hypothesis that methylation reactions at C-7 and C-8 are mutually exclusive. The unprecedented feature of C-5 methylation by *Ct*MenK was surprising and it cannot be excluded that this was due to a side reaction in the heterologous host, which may not occur in *C. tanakaei* cells. Furthermore, methylation at C-8 appeared to precede that at C-5 arguing that MenK might accept 8-MMK as an alternative substrate with a lower affinity and/or turnover rate compared to MK, which is likely due to the different orientation of the naphthoquinone head group in the active site.

What is the structural basis for the specific methylation at C-8 or C-7 of MK/DMK (or MMK/MDMK)? Remarkably, all three tested enzymes seem to methylate DMK in the same way as MK in *E. coli* suggesting that the C-2 methyl group is not involved in accepting the substrate. These findings are in line with the fact that *A. equolifaciens* also methylated MK_8 and DMK_8 when produced in *E. coli* cells (Hein *et al*., 2017). The homology models presented in Fig. 5 suggest that the head group of MK, DMK (or MMK) species is able to enter an assumed naphthoquinone binding pocket that is lined by SAM2 and a conserved hydrophobic residue (Y286 of *Ct*MenK or F288 of *Ct*MenK2) that possibly interacts with the naphthoquinone head group by pi stacking (Fig. 5B and C). The residues of the signature motif QxTxYPLx that distinguishes MqnK/MenK from MenK2 enzymes are located adjacently and the crucial tyrosine residue could play a role in the exact positioning of SAM2 and thus of its methyl group carbon atom that is eventually transferred to either C-7 or C-8 of the naphthoquinone. Interestingly, the QxTxYPLx motif is situated in the linker domain of the enzyme that has been shown before to play a decisive role in determining the specificity for C-8 or C-7 methylation as concluded from the production of several chimeric enzymes that consisted of *A. equolifaciens* MenK and MenK2 fragments (Hein *et al*., 2018).

Implications on microbiomes and possible application in synthetic biology

There is a huge discrepancy between the number of organisms that contain a putative (methyl)menaquinone methyltransferase-encoding gene and the number of organisms for which the formation of at least one MMK or DMMK species has been experimentally confirmed (Fig. 3; Supporting Information Tables S1 and S2). Since the actual composition of the quinone/quinol pool depends on the growth conditions, the MMK/DMMK production capacity might have been often overlooked in laboratory cultures grown under standard conditions, for example, during aerobiosis in a complex medium. Regularly, however, these conditions do not accurately reflect the natural habitat in terms of nutrient supply and the fact that native cells live and interact within a microbial community. Using the presented signature motifs of (methyl)menaquinone methyltransferases, this study offers the opportunity to assess the capacity of MMK/DMMK formation from metagenomic data. Furthermore, it enables the design of PCR primer pairs with the aim to discriminate the *mqnK*/*menK*/*menK2* genes from other genes encoding radical SAM enzymes such as *hemN*. The presence and function of MMK and DMMK in natural habitats like the human gut or the rumen are largely unclear, but it cannot be excluded that these compounds play a role in health and disease. Since the redox potentials of MMK/$MMKH_2$ and DMMK/$DMMKH_2$ are more negative than that of the MK/MKH_2 pair, the methylated MK derivatives are suitable to serve in dedicated electron transport chains that could, for example, transfer electrons to low-potential (and often toxic) sulfur compounds such as sulfite and polysulphides in anaerobic respiration (see Introduction). In this context, it is notable that the genomes of many Actinobacteria including the gut bacterium *A. equolifaciens* encode an unusually high number of complex iron–sulfur molybdoenzymes whose cellular function cannot be assigned by evaluating protein sequences alone (Rothery and Weiner, 2015; Hein *et al*., 2018). Such enzymes are often predicted to employ a PsrC-type quinone/quinol-reactive membrane anchor protein, homologues of which are used, for example, in electron transport to polysulfide- and sulfite-reducing enzymes (Eller *et al*., 2019). In general, members of the class Coriobacteriia occur in the intestinal tract of mammals and have been associated with diseases. Some species of the genera *Atopobium*, *Olsenella* and *Cryptobacterium* are thought to be responsible for periodontal and endodontic infections while some *Eggerthella* species have been reported to be involved in chronic inflammatory bowel diseases and bacteremia (Lau

et al., 2004; Copeland *et al*., 2009; Mavrommatis *et al*., 2009; Göker *et al*., 2010; Thota *et al*., 2011).

Together with our previous studies, we have shown that the quinone/quinol pool of *E. coli* and other genetically tractable bacteria can be engineered in various ways upon the expression of one or more *mqnK*/*menK*/*menK2* genes (Hein *et al*., 2017, 2018). Therefore, by using these tools in a Synthetic Biology approach, the future tailor-made composition of the quinone/quinol is conceivable. This could enable researchers to specifically adapt the quinone/quinol pool to the necessities of desirable biotechnological pathways that require the presence of low-potential MK derivatives.

Experimental procedures

Bacterial strains and culture conditions

All bacterial strains and mutants used in this study are listed in Table 2. *Escherichia coli* XL-1-Blue cells grown aerobically at 37°C in LB broth (Lennox) were used for standard plasmid propagation. Derivatives of *E. coli* BL21 (DE3) cells were used for the heterologous production of MenK or MenK2 proteins. For enzyme production, cells were grown aerobically at 37°C in a 2 l-flask with 0.5 l TB medium to an OD_{600} of 3. Subsequently, gene expression was induced with isopropyl-β-D-thiogalactopyranoside (IPTG; final concentration 0.25 mM), and Fe(III)citrate (final concentration 0.25 mM) and L-cysteine (final concentration 0.5 mM) were added. Cells were incubated for 2 days at 30°C under agitation (130 rpm) resulting in semi-aerobic conditions. Where appropriate, chloramphenicol (25 mg l^{-1}), spectinomycin (50 mg l^{-1}) or anhydrotetracycline (0.1 mg l^{-1}) were added.

Construction of E. coli *BL21 (DE3) Δ*ubiE

The deletion of *ubiE* in *E. coli* BL21 (DE3) cells was achieved using the Scarless Cas9 Assisted Recombineering (no-SCAR) system (Reisch and Prather, 2015, 2017). This approach is based on the λ-Red system for recombination combined with the introduction of Cas9-mediated double-strand breaks for selection, thereby allowing marker-free and scarless genome editing. *E. coli* BL21 (DE3) cells were transformed with pCas9-CR4 (Addgene, plasmid #62655) and subsequently with pKDsgRNA-ubiE (see below). The resulting cells were plated on LB agar containing spectinomycin and chloramphenicol and incubated over night at 30°C. Plasmid pCas9-CR4 harboured the chloramphenicol resistance gene and the *cas9* gene under control of a tetracycline-inducible promoter. Plasmid pKDsgRNA-ubiE was a derivative of pKDsgRNA-p15 (Addgene, plasmid #62656) harbouring the temperature-sensitive pSC101 ori, the spectinomycin resistance gene, a tetracycline-inducible sgRNA and the arabinose-inducible λ-Red operon encoding the three components Exo, Beta and Gam. The employed *ubiE* specific sgRNA (5'-GTATGTTCAGGCGAACGCTG-3′) for Cas9 targeting

Table 2. Bacterial strains and mutants used in this study.

Strain/mutant	Relevant properties[a]	Reference
Collinsella tanakaei		
1. Wild-type	Type strain DSM 22478^T	DSMZ
Ferrimonas marina		
2. Wild-type	Type strain DSM 16917^T	DSMZ
Escherichia coli		
3. XL1-Blue	*end*A1 *gyr*A96(*nal*^{R}) *thi*-1 *rec*A1 *rel*A1 *lac gln*V44 F′[::Tn10 *pro*AB$^+$ *lac*I^q Δ(*lac*Z)M15] *hsd*R17(r_K^- m_K^+)	Agilent Technologies
4. K-12 MG1655	F^- λ^- *ilvG*$^-$ *rfb*-50 *rph*-1	DSMZ
5. BL21 (DE3)	*fhuA2 [lon] ompT gal (λDE3) [dcm] ΔhsdS λ DE3 = λ sBamHIo ΔEcoRI-B int::(lacI::PlacUV5::T7 gene1) i21 Δnin5*	Agilent Technologies
6. BL21 (DE3) Δ*ubiE*	Derivative of strain 5 lacking the *ubiE* gene encoding a C-methyltransferase involved in ubiquinone and menaquinone biosynthesis	This work
7. *Fm*MenK	Derivative of strain 5 containing plasmid pAC-F647 that encodes *F. marina* MenK; Cm^R	This work
8. *Fm*975	Derivative of strain 5 containing plasmid pAC-F975 that encodes protein WP_073325975 from *F. marina*; Cm^R	This work
9. *Ct*MenK	Derivative of strain 5 containing plasmid pAC-C032 that encodes *C. tanakaei* MenK; Cm^R	This work
10. *Ct*MenK2	Derivative of strain 5 containing plasmid pAC-C643 that encodes *C. tanakaei* MenK2; Cm^R	This work
11. Δ*ubiE* *Fm*MenK	Derivative of strain 6 containing plasmid pAC-F647 that encodes *F. marina* MenK; Cm^R	This work
12. Δ*ubiE* *Ct*MenK	Derivative of strain 6 containing plasmid pAC-C032 that encodes *C. tanakaei* MenK; Cm^R	This work
13. Δ*ubiE* *Ct*MenK2	Derivative of strain 6 containing plasmid pAC-C643 that encodes *C. tanakaei* MenK2; Cm^R	This work

[a]Cm^R denotes resistance against chloramphenicol.

covered the first 20 bases of a protospacer adjacent motif (PAM) (5'-NGG-3′) in the *ubiE* gene. The primer pairs PS_ubiE_F/PS_ubiE_R and CPEC2F/gamR (Supporting Information Table S3) were used to replace the p15A sgRNA sequence with the *ubiE* sgRNA sequence. The two resulting fragments were combined by circulating polymerase extension cloning (CPEC) (Quan and Tian, 2011) to obtain the counterselection plasmid pKDsgRNA-ubiE. Furthermore, two DNA fragments were amplified from the genome of *E. coli* K-12 MG1655 cells by PCR using the primer pairs ubiE_FFA_F/ubiE_FFA_R and ubiE_RFA_F/ubiE_RFA_R (Supporting Information Table S3). The PCR products contained flanking regions of *ubiE* and overhangs complementary to each other. The two amplicons were ligated by CPEC and the sequence of the ligation product was confirmed by sequencing. This fragment served as the linear double-stranded donor DNA fragment for recombination.

For the construction of *E. coli* BL21 (DE3) Δ*ubiE*, *E. coli* BL21 (DE3) cells harbouring pCas9cr4 and pKDsgRNA-ubiE were cultivated in SOB medium with chloramphenicol and spectinomycin at 30°C. For the induction of the λ-Red system, 1.2% (w/v) L-arabinose was added and, after 1 h of incubation, the cells were made electrocompetent using glycerol/mannitol density step centrifugation (Warren, 2011). After electroporation (1-mm electroporation cuvette, 1.8 kV, 200 Ω and 25 μF) with the linear donor DNA fragment (300 ng), cells were recovered in SOC medium with 1.2% L-arabinose. The cells were incubated for 3 days at 30°C on LB agar in the presence of chloramphenicol, spectinomycin and anhydrotetracycline and the desired deletion of *ubiE* was confirmed by colony PCR. Subsequently, the mutant cells were cured from plasmid pKDsgRNA-ubiE by cultivation at 37°C making use of its temperature-sensitive pSC101 ori. The resulting cells were transformed with pKDsgRNA-p15 and incubated in the presence of anhydrotetracycline at 30°C, which resulted in Cas9-driven cutting of pCas9-CR4. Finally, pKDsgRNA-p15 was removed from the resulting cells by a temperature shift to 37°C.

Construction of plasmids for the expression of menK *or* menK2 *genes*

PCR for cloning and sequencing work was carried out using Q5 High Fidelity DNA polymerase (New England Biolabs). PCR-fragments and plasmids were purified using the GenElute HP Plasmid Mini or PCR Clean-Up Kit (Sigma-Aldrich). Four potential (methyl)menaquinone methyltransferase genes were amplified by PCR using cells of *Ferrimonas marina* or *Collinsella tanakaei* as template (Table 2) and respective primer pairs (Supporting Information Table S3). The genes from *C. tanakaei* encoded the proteins *Ct*MenK (WP_009142032) and *Ct*MenK2 (WP_009141643) while those from *F. marina* encoded *Fm*MenK (WP_067659647) and *Fm*975 (WP_073325975), respectively. Purified PCR products were ligated with a suitable PCR-amplified fragment of vector pACYCDuet-1 (Novagen) using the NEBuilder HiFi DNA Assembly Master Mix (New England Biolabs). The identity of the resulting plasmids pAC-C032, pAC-C643, pAC-F647 and pAC-F975 (Table 2) was confirmed by DNA sequencing (Seqlab, Göttingen, Germany).

Quinone extraction and analysis

E. coli cells were centrifuged at 10 000*g* for 10 min and suspended in 50 mM Tris/HCl (pH 8.0) buffer. The same volume of a mixture of methanol and petroleum benzene 60–70 (3:1, v/v) was added. After shaking at room temperature for 20 min, phases were separated by centrifugation at 3000*g* for 5 min. The quinone-containing petroleum phase was removed and the extraction was repeated. Subsequently, the petroleum was evaporated in a rotary vacuum concentrator. The quinone fraction was dissolved in petroleum, isopropanol and methanol (1:2:12, v/v) and separated by reversed phase high-pressure liquid chromatography (RP-HPLC). An OmniSpher 5 C18 150 × 4.6 mm column (Agilent Technologies) was used on a Hitachi LaChrom Elite system and a methanol/isopropanol solution (70:30; flow rate 1 ml min^{-1}) served as eluent. Quinones were detected using the L-2450 diode array detector at a wavelength of 248 nm and identified on the basis of their retention times and UV–Vis spectra as described earlier (Hein *et al*., 2017, 2018). For mass spectrometry (MS), samples were diluted in methanol and analysed by high-resolution MS using an Impact II instrument with atmospheric pressure chemical ionization as ion source (Bruker Daltonics).

Sequence database searches

A set of six MK methyltransferases and six further class C RSMTs was used in a PSI BLAST analysis of the non-redundant database at NCBI with the following settings: substitution matrix PAM250; gap existence cost 14; gap extension cost 2 and PSI-BLAST threshold 0.005 (Altschul *et al*., 1997). The 12 sequences were MenK and MenK2 from *Adlercreutzia equolifaciens* DSM 19450 (GenBank accession numbers BAN75994 and BAN76985, respectively), *Wolinella succinogenes* DSM 1740 MqnK (CAE09279), *Campylobacter jejuni* NCTC 11168 MqnK (CAL34513), *Thermoproteus tenax* Kra 1 MqnK (CCC80926), *Shewanella oneidensis* MR-1 MenK (AAN57484) as well as TpdI from *Nonomuraea* sp. Bp3714-39 (ACS83777), NosN from *Streptomyces*

actuosus ATCC 25421 (AWT44901), Blm-Orf8 from *Streptomyces verticillus* ATCC15003 (AAG02372), Jaw5 from *Streptomyces roseoverticillatus* HP-891 (BAO98806), YtkT from *Streptomyces* sp. TP-A0356 (ADZ13556) and C10P from *Streptomyces zelensis* NRRL 11183 (ARK19493).

Sequence clustering

To identify MK methyltransferases, CLANS (CLuster ANalysis of Sequences) was used, a JAVA application based on the Fruchtman–Reingold graph layout algorithm for two- and three-dimensional visualization of pairwise similarities between and within protein families (Frickey and Lupas, 2004). Attractive and repulsive forces between each sequence pair were calculated in proportion to the negative logarithm of the of high-scoring segment pairs (HSPs) *P*-values from an all-against-all BLAST. A three-dimensional graph was achieved by random positioning of the sequences in space followed by adjustment of the sequences according to the force vectors until the equilibrium state of the system was reached. Network-based clustering was applied to classify the protein families in the graph. The *P*-value cut off was set to 10^{-45} or, for subclusters, to 10^{-80}.

Sequence alignments and phylogenetic trees

Clustered amino acid sequences were extracted from CLANS and aligned using ClustalOmega 1.2.2 command-line version (Sievers and Higgins 2018). To define consensus sequences, amino acid positions identical in >95% of the sequences from the respective cluster were considered and specific motifs were identified manually. For the generation of the phylogenetic tree of HemN-like class C RSMTs, amino acid sequences were aligned using ClustalX 2.1 (Larkin *et al*., 2007). The software MrBayes (Ronquist *et al*., 2012) was used for Bayesian inference and the phylogenetic model. The amino acid analysis was integrated over a mixed set of evolutionary models (Poisson, JTT, Dayhoff, MtREV, MtMam, WAG, rtREV, cpREV, VT and BLOSUM). Two parallel runs were started, each consisting of six chains using Metropolis coupling (five hot and one cold). The number of generations was set to 1 000 000 for the Markov chain Monte Carlo analysis and the run diagnostics were computed every 100th generation. The number of discrete categories used to approximate the gamma distribution was set to 8. HemN was defined as outgroup. Subsequently, the two runs converged onto the stationary distribution with an average split frequency standard deviation of <0.01. Phylogenetic trees were drawn with iTOL (Letunic and Bork, 2016).

The phylogenetic tree of the MqnK/MenK/MenK2 family was constructed using programs of the PHYLIP 3.695 package (Felsenstein, 1989). The multiple sequence alignment was calculated with ClustalX 2.1. Bootstrapping was performed using *seqboot* with 1000 bootstrap replications. The consensus distance tree was constructed using *protdist* with the Jones–Taylor–Thornton model, *neighbour*, and *consense* with the Majority rule.

Homology modelling

Modelling of MK methyltransferase structures was performed using the SWISS-MODEL Server (Waterhouse *et al*., 2018). The crystal structure of *E. coli* HemN served as template (Layer *et al*., 2003). PyMOL v2.2.3 (Schrödinger, LLC.) was used to visualize and compare the homology models.

Acknowledgements

The authors thank Alexander Schießer and Christiane Rudolph for their help with mass spectrometric analyses. This work was supported by the Deutsche Forschungsgemeinschaft (project number 245761862 to J.S.).

References

Abicht, H.K., Martinez, J., Layer, G., Jahn, D., and Solioz, M. (2012) *Lactococcus lactis* HemW (HemN) is a haem-binding protein with a putative role in haem trafficking. *Biochem J* **442**: 335–343.

Altschul, S.F., Madden, T.L., Schaffer, A.A., Zhang, J., Zhang, Z., Miller, W., and Lipman, D.J. (1997) Gapped BLAST and PSI-BLAST: a new generation of protein database search programs. *Nucleic Acids Res* **25**: 3389–3402.

Broderick, J.B., Duffus, B.R., Duschene, K.S., and Shepard, E.M. (2014) Radical S-adenosylmethionine enzymes. *Chem Rev* **114**: 4229–4317.

Burkhart, B.J., Schwalen, C.J., Mann, G., Naismith, J.H., and Mitchell, D.A. (2017) YcaO-dependent posttranslational amide activation: biosynthesis, structure, and function. *Chem Rev* **117**: 5389–5456.

Copeland, A., Sikorski, J., Lapidus, A., Nolan, M., Del Rio, T. G., Lucas, S., *et al*. (2009) Complete genome sequence of *Atopobium parvulum* type strain (IPP 1246). *Stand Genomic Sci* **1**: 166–173.

Collins, M.D., and Jones, D. (1981) Distribution of isoprenoid quinone structural types in bacteria and their taxonomic implications. *Microbiol Rev* **45**: 481.

Dairi, T. (2012) Menaquinone biosyntheses in microorganisms. *Methods Enzymol* **515**: 107–122.

Dietrich, W., and Klimmek, O. (2002) The function of methylmenaquinone-6 and polysulfide reductase membrane anchor (PsrC) in polysulfide respiration of *Wolinella succinogenes*. *Eur J Biochem* **269**: 1086–1095.

Ding, Y., Yu, Y., Pan, H., Guo, H., Li, Y., and Liu, W. (2010) Moving posttranslational modifications forward to biosynthesize the glycosylated thiopeptide nocathiacin I in *Nocardia* sp. ATCC202099. *Mol Biosyst* **6**: 1180–1185.

Du, L., Sánchez, C., Chen, M., Edwards, D.J., and Shen, B. (2000) The biosynthetic gene cluster for the antitumor drug bleomycin from *Streptomyces verticillus* ATCC15003 supporting functional interactions between nonribosomal peptide synthetases and a polyketide synthase. *Chem Biol* **7**: 623–642.

Eller, J., Hein, S., and Simon, J. (2019) Significance of MccR, MccC, MccD, MccL and 8-methylmenaquinone in sulfite respiration of *Wolinella succinogenes*. *Biochim Biophys Acta Bioenerg* **1860**: 12–21.

Felsenstein, J. (1989) PHYLIP-phylogeny inference package (Ver. 3.2). *Cladistics* **5**: 164–166.

Frickey, T., and Lupas, A. (2004) CLANS: a Java application for visualizing protein families based on pairwise similarity. *Bioinformatics* **20**: 3702–3704.

Galm, U., Wendt-Pienkowski, E., Wang, L., George, N.P., Oh, T.-J., Yi, F., *et al*. (2009) The biosynthetic gene cluster of zorbamycin, a member of the bleomycin family of antitumor antibiotics, from *Streptomyces flavoviridis* ATCC 21892. *Mol Biosyst* **5**: 77–90.

Göker, M., Held, B., Lucas, S., Nolan, M., Yasawong, M., Glavina Del Rio, T., *et al*. (2010) Complete genome sequence of *Olsenella uli* type strain (VPI D76D-27C). *Stand Genomic Sci* **3**: 76–84.

Hein, S., Klimmek, O., Polly, M., Kern, M., and Simon, J. (2017) A class C radical *S*-adenosylmethionine methyltransferase synthesizes 8-methylmenaquinone. *Mol Microbiol* **104**: 449–462.

Hein, S., von Irmer, J., Gallei, M., Meusinger, R., and Simon, J. (2018) Two dedicated class C radical *S*-adenosylmethionine methyltransferases concertedly catalyse the synthesis of 7,8-dimethylmenaquinone. *Biochim Biophys Acta Bioenerg* **1859**: 300–308.

Hiratsuka, T., Furihata, K., Ishikawa, J., Yamashita, H., Itoh, N., Seto, H., and Dairi, T. (2008) An alternative menaquinone biosynthetic pathway operating in microorganisms. *Science* **321**: 1670–1673.

Homuth, G., Rompf, A., Schumann, W., and Jahn, D. (1999) Transcriptional control of *Bacillus subtilis* hemN and hemZ. *J Bacteriol* **181**: 5922–5929.

Huang, W., Xu, H., Li, Y., Zhang, F., Chen, X.-Y., He, Q.-L., *et al*. (2012) Characterization of yatakemycin gene cluster revealing a radical *S*-adenosylmethionine dependent methyltransferase and highlighting spirocyclopropane biosynthesis. *J Am Chem Soc* **134**: 8831–8840.

Ji, X., Mo, T., Liu, WQ., Ding, W., Deng, Z., and Zhang, Q. (2019). Revisiting the mechanism of the anaerobic coproporphyrinogen III oxidase HemN. *Angew Chem Int Ed* **58**: 6235–6238.

Jin, W.-B., Wu, S., Jian, X.-H., Yuan, H., and Tang, G.-L. (2018) A radical *S*-adenosyl-L-methionine enzyme and a methyltransferase catalyze cyclopropane formation in natural product biosynthesis. *Nat Commun* **9**: 2771.

Katsuta, A., Adachi, K., Matsuda, S., Shizuri, Y., and Kasai, H. (2005) *Ferrimonas marina* sp. nov. *Int J Syst Evol Microbiol* **55**: 1851–1855.

LaMattina, J.W., Nix, D.B., and Lanzilotta, W.N. (2016) Radical new paradigm for heme degradation in *Escherichia coli* O157:H7. *Proc Natl Acad Sci U.S.A* **113**: 12138–12143.

Larkin, M.A., Blackshields, G., Brown, N.P., Chenna, R., McGettigan, P.A., McWilliam, H., *et al*. (2007) Clustal W and Clustal X version 2.0. *Bioinformatics* **23**: 2947–2948.

Lau, S.K., Woo, P.C., Fung, A.M., Chan, K.M., Woo, G.K., and Yuen, K.Y. (2004) Anaerobic, non-sporulating, Gram-positive bacilli bacteraemia characterized by 16S rRNA gene sequencing. *J Med Microbiol* **53**: 1247–1253.

Layer, G., Moser, J., Heinz, D.W., Jahn, D., and Schubert, W.D. (2003) Crystal structure of coproporphyrinogen III oxidase reveals cofactor geometry of radical SAM enzymes. *EMBO J* **22**: 6214–6224.

Layer, G., Pierik, A.J., Trost, M., Rigby, S.E., Leech, H.K., Grage, K., *et al*. (2006) The substrate radical of *Escherichia coli* oxygen-independent coproporphyrinogen III oxidase HemN. *J Biol Chem* **281**: 15727–15734.

Lee, P.T., Hsu, A.Y., Ha, H.T., and Clarke, C.F. (1997) A C-methyltransferase involved in both ubiquinone and menaquinone biosynthesis: isolation and identification of the *Escherichia coli ubiE* gene. *J Bacteriol* **179**: 1748–1754.

Letunic, I., and Bork, P. (2016) Interactive tree of life (iTOL) v3: an online tool for the display and annotation of phylogenetic and other trees. *Nucleic Acids Res* **44**: W242–W245.

MacMillan, K.S., and Boger, D.L. (2009) Fundamental relationships between structure, reactivity, and biological activity for the duocarmycins and CC-1065. *J Med Chem* **52**: 5771–5780.

Mahanta, N., Zhang, Z., Hudson, G.A., van der Donk, W.A., and Mitchell, D.A. (2017) Reconstitution and substrate specificity of the radical *S*-adenosyl-methionine thiazole *C*-methyltransferase in thiomuracin biosynthesis. *J Am Chem Soc* **139**: 4310–4313.

Maruo, T., Sakamoto, M., Ito, C., Toda, T., and Benno, Y. (2008) *Adlercreutzia equolifaciens* gen. nov., sp. nov., an equol-producing bacterium isolated from human faeces, and emended description of the genus *Eggerthella*. *Int J Syst Evol Microbiol* **58**: 1221–1227.

Mavrommatis, K., Pukall, R., Rohde, C., Chen, F., Sims, D., Brettin, T., *et al*. (2009) Complete genome sequence of *Cryptobacterium curtum* type strain (12-3). *Stand Genomic Sci* **1**: 93–100.

Morris, R.P., Leeds, J.A., Naegeli, H.U., Oberer, L., Memmert, K., Weber, E., *et al*. (2009) Ribosomally synthesized thiopeptide antibiotics targeting elongation factor Tu. *J Am Chem Soc* **131**: 5946–5955.

Nagai, F., Watanabe, Y., and Morotomi, M. (2010) *Slackia piriformis* sp. nov. and *Collinsella tanakaei* sp. nov., new members of the family Coriobacteriaceae, isolated from human faeces. *Int J Syst Evol Microbiol* **60**: 2639–2646.

Nowicka, B., and Kruk, J. (2010) Occurrence, biosynthesis and function of isoprenoid quinones. *Biochim Biophys Acta Bioenerg* **1797**: 1587–1605.

Parish, T., Schaeffer, M., Roberts, G., and Duncan, K. (2005) HemZ is essential for heme biosynthesis in *Mycobacterium tuberculosis*. *Tuberculosis* **85**: 197–204.

Quan, J., and Tian, J. (2011) Circular polymerase extension cloning for high-throughput cloning of complex and combinatorial DNA libraries. *Nat Protoc* **6**: 242–251.

Reisch, C.R., and Prather, K.L.J. (2015) The no-SCAR (Scarless Cas9 assisted Recombineering) system for genome editing in *Escherichia coli*. *Sci Rep* **5**: 15096.

Reisch, C.R., and Prather, K.L.J. (2017) Scarless Cas9 assisted recombineering (no-SCAR) in *Escherichia coli*, an easy-to-use system for genome editing. *Curr Protoc Mol Biol* **117**: 31.38.31–31.38.20.

Ronquist, F., Teslenko, M., van der Mark, P., Ayres, D.L., Darling, A., Höhna, S., *et al*. (2012) MrBayes 3.2: efficient Bayesian phylogenetic inference and model choice across a large model space. *Syst Biol* **61**: 539–542.

Rothery, R.A., and Weiner, J.H. (2015) Shifting the metallocentric molybdoenzyme paradigm: the importance of pyranopterin coordination. *J Biol Inorg Chem* **20**: 349–372.

Schmid, R., Goebel, F., Warnecke, A., and Labahn, A. (1999) Synthesis and redox potentials of methylated vitamin K derivatives. *J Chem Soc Perkin Trans* **2**: 1199–1202.

Schnoes, A.M., Brown, S.D., Dodevski, I., and Babbitt, P.C. (2009) Annotation error in public databases: misannotation of molecular function in enzyme superfamilies. *PLoS Comput Biol* **5**: e1000605.

Sievers, F., and Higgins, D.G. (2018) Clustal omega for making accurate alignments of many protein sequences. *Protein Sci* **27**: 135–145.

Sofia, H.J., Chen, G., Hetzler, B.G., Reyes-Spindola, J.F., and Miller, N.E. (2001) Radical SAM, a novel protein superfamily linking unresolved steps in familiar biosynthetic pathways with radical mechanisms: functional characterization using new analysis and information visualization methods. *Nucleic Acids Res* **29**: 1097–1106.

Tao, M., Wang, L., Wendt-Pienkowski, E., George, N.P., Galm, U., Zhang, G., *et al*. (2007) The tallysomycin biosynthetic gene cluster from *Streptoalloteichus hindustanus* E465-94 ATCC 31158 unveiling new insights into the biosynthesis of the bleomycin family of antitumor antibiotics. *Mol Biosyst* **3**: 60–74.

Thota, V.R., Dacha, S., Natarajan, A., and Nerad, J. (2011) *Eggerthella lenta* bacteremia in a Crohn's disease patient after ileocecal resection. *Future Microbiol* **6**: 595–597.

Tocchetti, A., Maffioli, S., Iorio, M., Alt, S., Mazzei, E., Brunati, C., *et al*. (2013) Capturing linear intermediates and C-terminal variants during maturation of the thiopeptide GE2270. *Chem Biol* **20**: 1067–1077.

Unden, G., and Bongaerts, J. (1997) Alternative respiratory pathways of *Escherichia coli*: energetics and transcriptional regulation in response to electron acceptors. *Biochim Biophys Acta Bioenerg* **1320**: 217–234.

Wang, J., Woldring, R.P., Román-Meléndez, G.D., McClain, A.M., Alzua, B.R., and Marsh, E.N.G. (2014) Recent advances in radical SAM enzymology: new structures and mechanisms. *ACS Chem Biol* **9**: 1929–1938.

Warren, D.J. (2011) Preparation of highly efficient electrocompetent *Escherichia coli* using glycerol/mannitol density step centrifugation. *Anal Biochem* **413**: 206–207.

Watanabe, H., Tokiwano, T., and Oikawa, H. (2006a). Biosynthetic study of FR-900848: origin of the aminodeoxynucleoside part. *J Antibiot* **59**: 607–610.

Watanabe, H., Tokiwano, T., and Oikawa, H. (2006b). Biosynthetic study of FR-900848: unusual observation on polyketide biosynthesis that did not accept acetate as origin of acetyl-CoA. *Tetrahedron Lett* **47**: 1399–1402.

Waterhouse, A., Bertoni, M., Bienert, S., Studer, G., Tauriello, G., Gumienny, R., *et al*. (2018) SWISS-MODEL: homology modelling of protein structures and complexes. *Nucleic Acids Res* **46**: W296–W303.

Wu, S., Jian, X.-H., Yuan, H., Jin, W.-B., Yin, Y., Wang, L.-Y., *et al*. (2017) Unified biosynthetic origin of the benzodipyrrole subunits in CC-1065. *ACS Chem Biol* **12**: 1603–1610.

Yu, Y., Duan, L., Zhang, Q., Liao, R., Ding, Y., Pan, H., *et al*. (2009) Nosiheptide biosynthesis featuring a unique indole side ring formation on the characteristic thiopeptide framework. *ACS Chem Biol* **4**: 855–864.

Zhang, Z., Mahanta, N., Hudson, G.A., Mitchell, D.A., and van der Donk, W.A. (2017) Mechanism of a class C radical *S*-adenosyl-l-methionine thiazole methyl transferase. *J Am Chem Soc* **139**: 18623–18631.

Supporting Information

Additional Supporting Information may be found in the online version of this article at the publisher's web-site:

Appendix S1: Supplementary Information